Contents lists available at SciVerse ScienceDirect

CIRP Annals Manufacturing Technology

Journal homepage: www.elsevier.com/locate/cirp

Integrated design of a 4-DOF high-speed pick-and-place parallel robot

Y.H. Li[a], Y. Ma[a], S.T. Liu[a], Z.J. Luo[a], J.P. Mei[a], T. Huang (1)[a,b,*], D.G. Chetwynd[b]

[a] *Key Laboratory of Mechanism Theory and Equipment Design of State Education Ministry, Tianjin University, Tianjin 300072, China*
[b] *School of Engineering, The University of Warwick, Coventry CV4 7AL, UK*

This paper draws on robotic mechanisms theory and elastic dynamics to propose a new methodology for the integrated design of a 4-DOF SCARA pick-and-place parallel robot. The design process, which is readily applied to other designs, is implemented by four interactive steps: (1) conceptual design and mechanical realization of the light-weight yet rigid articulated travelling plate; (2) dimensional synthesis by minimizing the maximum driving toque of a single actuated joint; (3) structural parameter design for achieving good elastic dynamic behaviours; and (4) motor sizing necessary to generate the specified cycle time. Based upon the proposed process a virtual prototype is designed for achieving a cycle time for up to 150 picks/min.

Parallel kinematics; Conceptual design; Computer aided design (CAD)

1. Introduction

Recently, pick-and-place parallel robots have been in ever increasing demands in the electronic, packaging, pharmaceutical and many other light industries. Most pick-and-place operations require SCARA or Schoenflies motions [1] having three translations and one rotation about a vertical axis. Two high-speed SCARA parallel robots are on the market, both using limbs containing proximal revolute actuated joints and parallelograms. The well-known Delta robot [2] has three identical R-(SS)^2 limbs and a fourth "telescope" RUPU limb for generating the vertical axis rotation. Here, R represents an actuated revolute joint, (SS)^2 denotes two spherical joints at either extremity of a spatial parallelogram, and U a universal joint. The Quattro robot [3] evolved from the Par4 employs four identical R-(SS)^2 limbs linked to an articulated platform that generates a rotation about the vertical axis by an angular amplification device. It is claimed that the four limbs design has potential to attain better transmission accuracy of the rotation and longer service life in comparison with the RUPU limb design.

The capability and efficiency of pick-and-place parallel robots relies not only upon the appropriate topological structures and right geometric dimensions but also upon the desirable elastic dynamic behaviours, sound trajectory planning and even upon the quality of the computer control. Therefore, it is crucially important to develop an integrated design process which can incorporate theory of robotic mechanisms [4] with CAD/CAE technology [5, 6]; proper virtual prototyping ensures the subsequent physical prototype can meet comprehensive performance requirements. A rigorous approach is presented.

Building on the idea of an articulated travelling plate and driven by many practical needs from the packaging industry, this paper considers a novel 4-DOF SCARA pick-and-place parallel robot. Integrated design involves: conceptual design and mechanical realization of a lightweight yet rigid articulated travelling plate; optimal parameter design for achieving good kinematic, rigid body as well as elastic dynamic behaviours simultaneously over the complete task workspace; and motor sizing necessary to generate the specific motions. The study is centred on designing a virtual prototype having a cycle time suitable for up to 150 picks/min (or a maximum acceleration of up to 15g).

2. Conceptual design

Figure 1(a) shows a 3D view of the proposed 4-DOF SCARA parallel robot under consideration. It has two identical closed-loop sub-chains, each consisting of two identical R-(SS)^2 limbs connected with the base at one end and with either subpart 1 or 2 of the travelling plate at the other. Subparts 1 and 2 are articulated by prismatic joints to subpart 3 as shown in Figure 1(c). Briefly, the desired Schoenflies motion subgroup of the articulated travelling plate is generated as follows. The axes of the two actuated R joints within a sub-chain are set orthogonal to each other. The entire set of accessible motions of subpart 1(2) then forms a Schoenflies motion subgroup having a rotation axis about $\boldsymbol{s}$, the cross product of two unit vectors $\boldsymbol{s}_1$ and $\boldsymbol{s}_2$, each normal to one parallelogram within the sub-chain as shown in Figure 1(b). By placing the two sub-chains with mirror symmetry, their axes can have common components only vertically or perpendicular to the mirroring plane. So, placing the prismatic joint of the articulated plate in the horizontal plane with its axis in the mirroring plane (i.e., at 45° to the parallelograms) restrains all rotations. The required rotation about the z axis is then generated from relative translation between subparts 1 and 2 *via* a rack-and-pinion assembly centred on subpart 3. The design

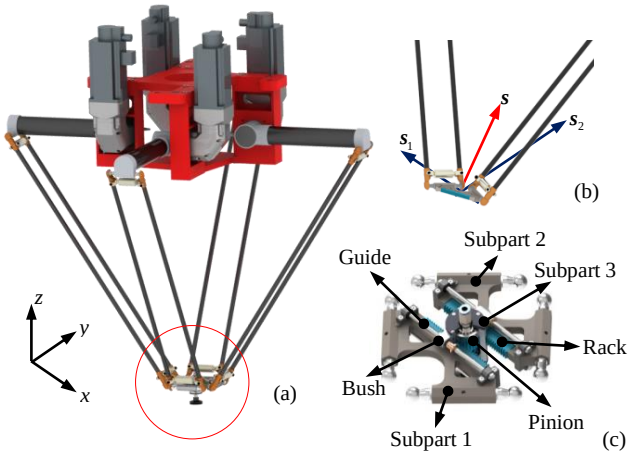

Figure 1. 3D view of the SCARA parallel robot

allows all three subparts to be compact and light-weight yet rigid; subparts 1 and 2 then travel smoothly relative to subpart 3 by using four small bushes acting along two pairs of hollow cylindrical guideways located on the top and bottom of subpart 1 and 2. Thus it ensures the transmission accuracy and rigidity of rotational motion about the *z* axis.

3. Kinematic and dynamic modelling

Having the topological structure of the SCARA parallel robot already to hand, kinematic, rigid body and elastic dynamic modelling and analyses are essential for the formulation of appropriate performance indices and constraints.

3.1. Kinematic and rigid body dynamic modelling

Inverse kinematic and rigid body dynamic analyses are concerned with the determination of the position angles, angular velocities/accelerations and driving toques of the upper arms necessary to generate the specific motions of the end-effector. Figure 2 shows the schematic diagram of the robot reflecting that the three subparts of the travelling plate undergo pure translation and the two rods within a parallelogram have identical motion. The loop closure constraint equation of the *i*th limb can be formulated by

$$\boldsymbol{t}_i - l_1\boldsymbol{u}_i - l_2\boldsymbol{w}_i = \boldsymbol{0},\ i=1,\ldots,4 \tag{1}$$

$$\boldsymbol{t}_i = \boldsymbol{L}_i\boldsymbol{x} - \boldsymbol{e}_i,\ \boldsymbol{L}_i = \begin{bmatrix}\boldsymbol{E}_3 & \varepsilon_i\hat{\boldsymbol{x}}\end{bmatrix},\ \boldsymbol{x} = \begin{pmatrix}\boldsymbol{r}\\ s\end{pmatrix}$$

$$\boldsymbol{e}_i = e\begin{pmatrix}\cos\gamma_i\\ \sin\gamma_i\\ 0\end{pmatrix},\ \gamma_i = (i-1)\pi/2+\pi/4,\ \varepsilon_i = \begin{cases}1 & i=1,2\\ -1 & i=3,4\end{cases}$$

where $\boldsymbol{r}$ is the position vector of point P on subpart 3 with s being the stroke of subpart i ($i=1,2$) relative to subpart 3 along the x axis; e is the offset from O to the rotary axis of a upper arm; γ_i is the position angle of the ith upper arm; l_1, l_2, $\boldsymbol{u}_i$, $\boldsymbol{w}_i$ are the lengths and unit vectors of the ith upper arm and connecting rod; E_3 is a 3×3 unity matrix.

Then, the kinematic analyses result in the inverse position velocity and acceleration models as follows.

$$\theta_i = 2\arctan\frac{-A_i+\sqrt{A_i^2+B_i^2-C_i^2}}{C_i-B_i},\ \dot{\boldsymbol{\theta}} = \boldsymbol{J}\dot{\boldsymbol{x}},\ \ddot{\boldsymbol{\theta}} = \boldsymbol{J}\ddot{\boldsymbol{x}}+\boldsymbol{h} \tag{2}$$

where

$$A_i = -2l_1\boldsymbol{t}_i^{\mathrm{T}}\hat{\boldsymbol{z}},\ B_i = -2l_1\boldsymbol{t}_i^{\mathrm{T}}\left(\cos\gamma_i\hat{\boldsymbol{x}}+\sin\gamma_i\hat{\boldsymbol{y}}\right),\ C_i = \boldsymbol{t}_i^{\mathrm{T}}\boldsymbol{t}_i + l_1^2 - l_2^2$$

$$\boldsymbol{J} = \boldsymbol{J}_q^{-1}\boldsymbol{J}_x,\ \boldsymbol{J}_q = l_1\mathrm{diag}\left[\Delta_i\right],\ \boldsymbol{J}_x = \begin{bmatrix}\boldsymbol{w}_1 & \boldsymbol{w}_2 & \boldsymbol{w}_3 & \boldsymbol{w}_4\\ \boldsymbol{w}_1^{\mathrm{T}}\hat{\boldsymbol{x}} & \boldsymbol{w}_2^{\mathrm{T}}\hat{\boldsymbol{x}} & -\boldsymbol{w}_3^{\mathrm{T}}\hat{\boldsymbol{x}} & -\boldsymbol{w}_4^{\mathrm{T}}\hat{\boldsymbol{x}}\end{bmatrix}^{\mathrm{T}}$$

$$\boldsymbol{h} = \begin{pmatrix}h_1\\ \vdots\\ h_4\end{pmatrix},\ h_i = \frac{1}{l_1^2\Delta_i^3}\dot{\boldsymbol{x}}^{\mathrm{T}}\boldsymbol{L}_i^{\mathrm{T}}\boldsymbol{H}_i\boldsymbol{L}_i\dot{\boldsymbol{x}},\ \Delta_i = \boldsymbol{w}_i^{\mathrm{T}}\left(\boldsymbol{v}_i\times\boldsymbol{u}_i\right)$$

$$\boldsymbol{H}_i = \begin{bmatrix}\left(\boldsymbol{v}_i\times\boldsymbol{u}_i\right)^{\mathrm{T}}\left(\boldsymbol{v}_i\times\boldsymbol{w}_i\right)\boldsymbol{w}_i\boldsymbol{w}_i^{\mathrm{T}}\\ +\Delta_i l_1/l_2\left(\Delta_i\boldsymbol{E}_3-(\boldsymbol{v}_i\times\boldsymbol{u}_i)\boldsymbol{w}_i^{\mathrm{T}}\right)^{\mathrm{T}}\left(\Delta_i\boldsymbol{E}_3-(\boldsymbol{v}_i\times\boldsymbol{u}_i)\boldsymbol{w}_i^{\mathrm{T}}\right)\end{bmatrix}$$

To formulate the inverse rigid body dynamics, assume that the moment of inertia of the rods within a parallelogram is negligible because of the light-weight design using carbon fibres. The mass of the arm is then divided into two lump masses at two endpoints according to the static equilibrium principle. Consequently, a simplified inverse dynamic model can be employed.

$$\boldsymbol{\tau} = \boldsymbol{\tau}_a + \boldsymbol{\tau}_v + \boldsymbol{\tau}_g \tag{3}$$

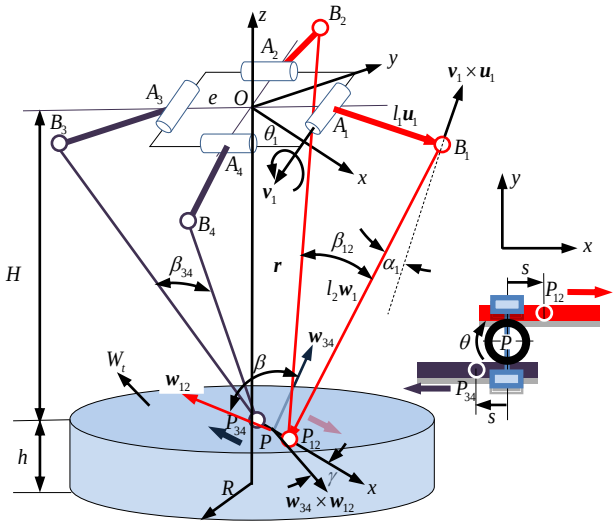

Figure 2. Kinematic diagram of the 4-DOF parallel robot

where $\boldsymbol{\tau}$ is the driving torque vector imposed upon the upper arms with $\boldsymbol{\tau}_a$, $\boldsymbol{\tau}_v$ and $\boldsymbol{\tau}_g$ being the inertial, centrifugal/Coriolis and gravitational components

$$\boldsymbol{\tau}_a = \left(\boldsymbol{J}^{-\mathrm{T}}\boldsymbol{m}+I_a\boldsymbol{J}\right)\ddot{\boldsymbol{x}},\ \boldsymbol{m} = \begin{bmatrix}\left(m_p+m_3\right)\boldsymbol{E}_3 & \\ & m_p+I_3/r^2\end{bmatrix}$$

$$\boldsymbol{\tau}_v = I_a\boldsymbol{h},\ \boldsymbol{\tau}_g = m_a r_a g\begin{pmatrix}\cos\theta_1\\ \vdots\\ \cos\theta_4\end{pmatrix} + \boldsymbol{J}^{-\mathrm{T}}\begin{pmatrix}\left(m_p+m_3\right)g\hat{\boldsymbol{z}}\\ 0\end{pmatrix}$$

m_p is the equivalent mass of subparts 1 and 2; m_3 and I_3 are the mass and moment of inertia of subpart 3 with r being the radius of the pinion; I_a and $m_a r_a$ are the equivalent moment of inertia and mass-radius product of a upper arm about its rotary axis.

3.2. Elastic dynamic modelling and analysis

Since the elastic dynamic behaviours vary with the design variables and system configurations, a rapid feature mapping from CAD to CAE is essential to ensure both the eigenvalue and transient analysis to be implemented in an effective manner. Working with SolidWorks and SAMCEF, we develop an interface (see Figure 3) using Bacon and Notebook embedded in SAMCEF.

(1) Create a CAD model of the robot using SolidWorks;
(2) Parameterize the geometrical and physical features of the CAD model in the Notebook format;
(3) Convert the physical features into the Bacon format readily for FE analysis;
(4) Evaluate the elastic dynamic behaviors by the FE solver in SAMCEF using the updated features extracted from a series of configurations.

In the physical features extraction, the spherical, revolute, prismatic joints as well as rack-and-pinion assembly used in the robot can be modeled by the contact elements provided by SAMCEF as shown in Figure 4, and the parameters of springs and dampers in these joint models can be specified using product catalogues, design handbooks and experimental measurements to ensure the simulation fidelity.

4. Integrated design

Equipped with the kinematic, rigid body and elastic dynamic models, the integrated design of the parallel robot can be carried out with two closely related missions: (1) determine a suite of dimensional and structural parameters of the moving links for

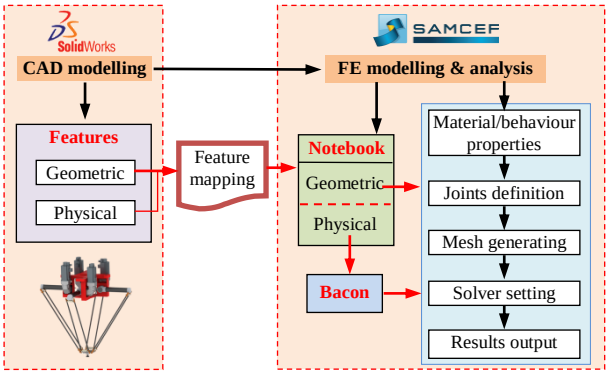

Figure 3. CAD/CAE based elastic dynamic modelling and analysis

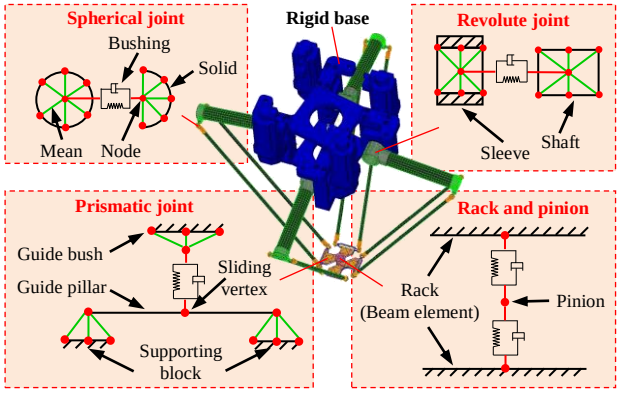

Figure 4. Joint modelling in FE analysis

achieving desirable kinematic and dynamic performance over the cylindrical workspace W_t of radius R and height h as shown in Figure 2; (2) specify the servomotor and gear reducer necessary to generate the specified motions.

4.1. Kinematic constraints

The determinants of $\boldsymbol{J}_q$ and $\boldsymbol{J}_x$ in Eq.(2) can be expressed as

$$\det(\boldsymbol{J}_q)=l_1^4\prod_{i=1}^{4}\Delta_{q,i}=l_1^4\prod_{i=1}^{4}\boldsymbol{w}_i^{\mathrm{T}}(\boldsymbol{v}_i\times\boldsymbol{u}_i)=l_1^4\prod_{i=1}^{4}\cos(\pi-\alpha_i)$$
$$\det(\boldsymbol{J}_x)=\Delta_x=\left((\boldsymbol{w}_1\times\boldsymbol{w}_2)\times(\boldsymbol{w}_3\times\boldsymbol{w}_4)\right)^{\mathrm{T}}\hat{\boldsymbol{x}}=\sin\beta_{12}\sin\beta_{34}\sin\beta\cos\gamma \quad (4)$$

Their geometrical meanings can be represented by a set of angles clearly depicted in Figure 2. Obviously, the serial singularity occurs when $\Delta_{q,i}\to 0\Leftrightarrow\alpha_i\to 90^\circ$ and the parallel singularity when $\Delta_x\to 0\Leftrightarrow\beta_{12}(\beta_{34})\to 0$ or $\beta\to 0$ or $\gamma\to 90^\circ$. Thus,

$$\min_{\boldsymbol{x}\in W_t}\min_{i=1,\ldots,4}\left|\Delta_{q,i}\right|\le\left[\Delta_q\right],\ \min_{\boldsymbol{x}\in W_t}\le\left[\Delta_x\right] \quad (5)$$

can be taken as the constraints to ensure the overall kinematic performance. The former is closely related to the speed and the latter to the accuracy of the end-effector. Here, $\left[\Delta_q\right]$ and $\left[\Delta_x\right]$ are the allowable minimum values over W_t.

4.2. Dynamic performance indices

The maximum value of the driving torque of the ith upper arm for generating $\|\ddot{\boldsymbol{x}}\|=1$ at a specific configuration can be represented by the maximum singular value $\sigma_{a,i\max}$ of the ith row of $\boldsymbol{G}_a=\boldsymbol{J}^{-\mathrm{T}}\boldsymbol{m}+I_a\boldsymbol{J}$ given in Eq(3), i.e.

$$\sigma_{a,i\max}\left(\boldsymbol{G}_{a,i}\right)=\sqrt{\boldsymbol{G}_{a,i}\boldsymbol{G}_{a,i}^{\mathrm{T}}},\ \boldsymbol{G}_{a,i}=\frac{l_1\Delta_i}{\Delta}\boldsymbol{J}_{x,i}^{*\mathrm{T}}\boldsymbol{m}+\frac{I_a}{l_1\Delta_i}\boldsymbol{J}_{x,i},\ i=1,\ldots,4 \quad (6)$$

where $\boldsymbol{J}_{x,i}$ and $\boldsymbol{J}_{x,i}^*$ are the ith row of $\boldsymbol{J}_x$ and its adjoint matrix. Note that $\sigma_{a,i\max}\to\infty$ if either the serial ($\Delta_i\to 0$) or the parallel ($\Delta\to 0$) singularity occurs. Thus, the maximum value out of four actuators over W_t should be minimized.

$$F_1=\max_{\boldsymbol{x}\in W_t}\max_{i=1,\ldots,4}\left(\sigma_{a,i\max}\left(\boldsymbol{G}_{a,i}\right)\right)\to\min \quad (7)$$

Similarly, the maximum driving torque of the ith upper arm for producing $\|\dot{\boldsymbol{x}}\|=1$ can be represented by the maximum singular value $\sigma_{v,i\max}$ of $\boldsymbol{G}_{v,i}=\left(I_a/l_1^2\Delta_i^3\right)\boldsymbol{L}_i^{\mathrm{T}}\boldsymbol{H}_i\boldsymbol{L}$. Thus, the maximum value out of four actuators over W_t should also be minimized.

$$F_2=\max_{\boldsymbol{x}\in W_t}\max_{i=1,\ldots,4}\left(\sigma_{v,i\max}\left(\boldsymbol{G}_{v,i}\right)\right)\to\ \min \quad (8)$$

Finally, to achieve a lightweight design with a high dynamic response, the reciprocal of the first order natural frequency at the centre of W_t *vs.* the total mass of the moving links can be considered as the third performance index for minimization.

$$F_3=\frac{M}{f_1}\to\min \quad (9)$$

4.3. Formulation of the optimal design problem

By taking dimensions e, l_1, l_2 and H, and cross sections of the upper arm and connecting rod as the design variables, a multi-objective optimization problem can be formulated

$$\chi\to\min \quad (10)$$

subject to

$$\boldsymbol{F}-(\chi+1)\boldsymbol{F}^*\le 0,\ \boldsymbol{F}^*=\left(\min F_1\quad \min F_2\quad \min F_3\right)^{\mathrm{T}}$$
$$\left[\Delta_x\right]-\min_{\boldsymbol{x}\in W_t}\left(\Delta_x\right)\le 0,\ \left[\Delta_q\right]-\min_{\boldsymbol{x}\in W_t}\min_{i=1,\ldots,4}\left(\left|\Delta_{q,i}\right|\right)\le 0$$
$$R-\left(e+l_1\right)=0,\ e_{\min}-e\le 0$$

The goal attainment algorithm within the Matlab Optimization Toolbox is readily available to solve this problem.

4.4. Design procedure

Considering the intensively interactive design tasks and the heavy computational burden in evaluating the elastic dynamic behaviours, the hierarchical design procedure is proposed:

(1) Select a reasonable initial moment of inertia and gear ratio for the reducer; specify the maximum acceleration and motion rule of the end-effector in pick-and-place operation;
(2) Discretize and parameterize the CAD features of a group of reasonable cross sections of the upper arm and connecting rod by SolidWorks;
(3) Determine a group of the optimized dimensions associated with those of the discrete structural parameters by solving the optimal problem given in Eq.(10) considering only F_1 and F_2;
(4) Evaluate F_3 by SAMCEF using the group of the optimized dimensions and the discrete structural parameters, and take the minimum one as the final solution;
(5) Determine the max/rated speed, torque, power and moment of inertia of the servomotor necessary to generate the motion specified by the Extended Adept Cycle [3];
(6) Examine the validity of the initially selected gear reducer's specifications.

5. An example of virtual prototyping

The procedure given in 4.4 is applied to the proposed parallel robot having a cylindrical task workspace of $R=0.5$ m and

$h = 0.25$ m. Given the gear reducers available on market and mechanical realization of the travelling plate, the fixed inertial parameters are set at

$$I_{\text{gear}} = 1.87\times10^{-4}\ \text{kg.m}^2,\ n = 20$$

$$m_{1(2)} = 0.52\ \text{kg},\ m_3 = 0.26\ \text{kg},\ I_3 = 0.032\times10^{-4}\ \text{kg.m}^2$$

We set $e_{\min} = 0.125$ m to retain room for installing servomotors; $[\Delta_x] = 1/4$ and $[\Delta_q] = \sqrt{2}/2$ ensure kinematic performance according to the geometric meanings of the angles in Figure 2.

Then, a suite of the optimized dimensions and cross sections can be found by implementing the procedure given in 4.3.

$$e = 0.125\ \text{m},\ l_1 = 0.375\ \text{m},\ l_2 = 0.950\ \text{m},\ H = 0.734\ \text{m}$$

$$D_{\text{arm}} = 60\ \text{mm},\ t_{\text{arm}} = 2.5\ \text{mm};\ D_{\text{rod}} = 16\ \text{mm},\ t_{\text{rod}} = 2.0\ \text{mm}$$

$$F_1 = 1.8584\ \text{N.s}^2,\ F_2 = 1.9338\ \text{N.s},\ F_3 = 0.3615\ \text{kg/Hz}$$

$$\min_{\boldsymbol{x}\in W_t} \Delta = 0.305,\ \min_{\boldsymbol{x}\in W_t} \min_{i=1,\ldots,4} \left(\left|\Delta_{q,i}\right|\right) = 0.707$$

Utilizing the 3-4-5 polynomial and the Extended Adept Cycle for trajectory planning, motor sizing to achieve a cycle time of 150picks/min results in the specifications shown in Table 1, and verifies the validity of the initially selected gear reducer.

Table 1
The servomotor specifications

P_{rated}	2 kW	I_{motor}	3.81×10^{-4} kg.m^2
N_{rated}	3000 rpm	τ_{rated}	6.36 N.m

Figure 5 shows the kinematic and rigid body dynamic performance indices across the middle layer of W_t, where the robot has better overall performance than in the top and bottom layers of the workspace. Figures 6 and 7 show the estimated first four natural frequencies in the middle layer of W_t and the corresponding mode shapes at the centre of the workspace. It is observed *via* simulation that the first two mode shapes dominate the dynamic positioning accuracy, while the fourth one dominates the dynamic rotational accuracy of the end-effector. Simulations also show that stiffness and damping of the gear reducers have significant effect on the residual vibration of the end-effector by exciting lower structural vibration frequencies. The dynamic positioning accuracy of the end-effort could be further improved by use of either a direct drive or an input shaping method [7].

6. Conclusions

An integrated design process is proposed that incorporates robotics theory with virtual prototyping. It achieves good and comprehensive performance simultaneously in kinematics and both rigid body and elastic dynamics.

As illustration, a lightweight yet rigid design for an articulated travelling plate is proposed, which helps to ensure the transmission accuracy and service life of the considered SCARA parallel robot. However, the technique is readily used elsewhere.

Given the promising results of the integrated design process, a test bench is being built for further experimental investigation and physical validation of the simulations. The results will be fully reported in due course.

Acknowledgement

The research is partially supported by the National Natural Science Foundation of China (Grant 51135008) and the National High Technology Research and Development Program of China (Grant 2013AA040501).

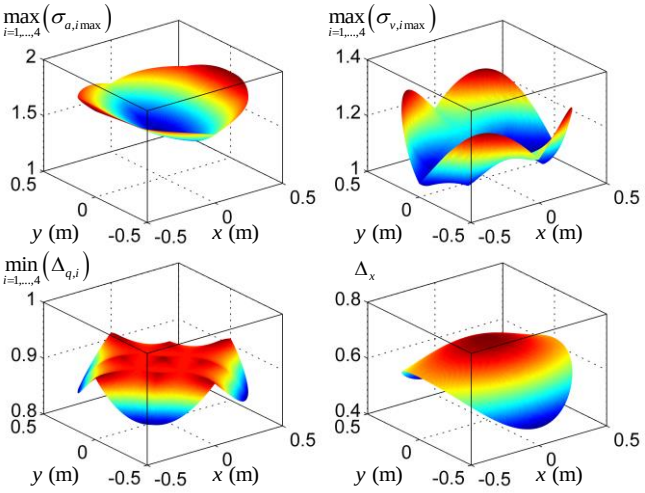

Figure 5. Distributions of kinematic and rigid body dynamic performance cross the middle layer of task workspace

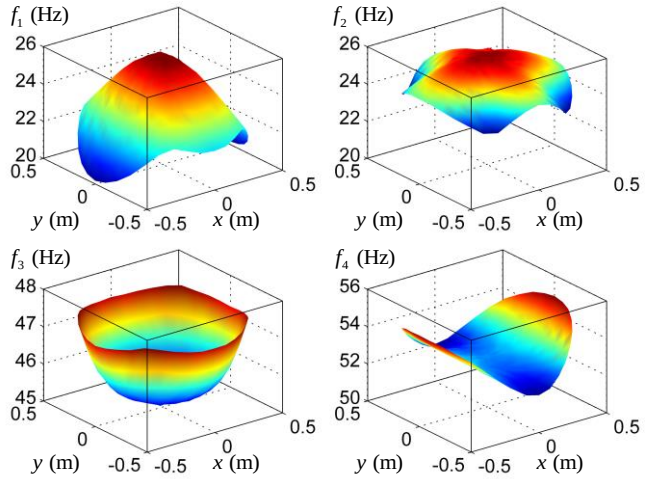

Figure 6. Distributions of natural frequencies cross the middle layer of task workspace

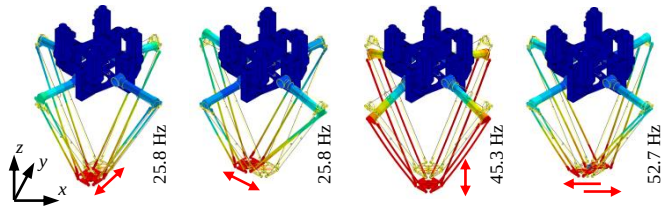

Figure 7. The first four mode shapes at the center of the workspace

References

[1] Hervé, J.M., 1999, The Lie Group of Rigid Body Displacements, A Fundamental Tool for Mechanism Design, Mech Mach Theory, 34/5:719–730.

[2] Clavel, R., 1988, Delta, A Fast Robot with Parallel Geometry, In Proceedings-18th Int Symp Industrial Robots:91-100, IFS publications, Lausanne.

[3] Pierrot, F., Nabat, V., Company, O., Krut, S., Poignet, P., 2009, Optimal Design of a 4-DOF Parallel Manipulator: From Academia to Industry, IEEE Trans on Robotics, 25/2:213-224.

[4] Tsai, L.W., 1999, Robot Analysis: The Mechanics of Serial and Parallel Manipulators, John Wiley, New York.

[5] Altintas, Y., Brecher, C., Weck, M., Witt, S., 2005, Virtual Machine Tool, Annals of the CIRP, 54/2:651-674.

[6] Brecher, C., Esser, M., Witt, S., 2009, Interaction of Manufacturing Process and Machine Tool, Annals of the CIRP, 58/2:588-607.

[7] Altintas, Y., Khoshdarregi, M.R., 2012, Contour Error Control of CNC Machine Tools with Vibration Avoidance, Annals of the CIRP, 61/1:335-338.